Investigation of spectral interferences on the accuracy of broadband CW-NIRS tissue SO_2 determination

Fengmei Zou,[1,*] Chunguang Jin,[1] Randy R. Ross,[2] and Babs Soller[1,3]

[1]*Department of Anesthesiology, University of Massachusetts Medical School, Worcester, MA, 01655, USA*
[2]*Department of Physics, College of the Holy Cross, Worcester, MA, 01610, USA*
[3]*Reflectance Medical Inc., Northboro, MA 01532, USA*
**Fengmei.Zou@umassmed.edu*

Abstract: An accurate SO_2 prediction method for using broadband continuous-wave diffuse reflectance near infrared (NIR) spectroscopy is proposed. The method fitted the NIR spectra to a Taylor expansion attenuation model, and used the simulated annealing method to initialize the nonlinear least squares fit. This paper investigated the effect of potential spectral interferences that are likely to be encountered in clinical use, on SO_2 prediction accuracy. The factors include the concentration of hemoglobin in blood, the volume of blood and volume of water in the tissue under the sensor, reduced scattering coefficient, μ_s', of the muscle, fat thickness and the source-detector spacing. The SO_2 prediction method was evaluated on simulated muscle spectra as well as on dual-dye phantoms which simulate the absorbance of oxygenated and deoxygenated hemoglobin.

OCIS codes: (170.0170) Medical optics and biotechnology; (170.1470) Blood/tissue constituent monitoring; (170.6510) Spectroscopy, tissue diagnostics; Muscle oxygen saturation measurement; Simulated annealing

References and links

1. M. Wolf, M. Ferrari, and V. Quaresima, "Progress of near-infrared spectroscopy and topography for brain and muscle clinical applications," J. Biomed. Opt. **12**(6), 062104 (2007).
2. J. M. Murkin, and M. Arango, "Near-infrared spectroscopy as an index of brain and tissue oxygenation," Br. J. Anaesth. **103**(6 Suppl 1), i3–i13 (2009).
3. E. Gerz, D. Geraskin, P. Neary, J. Franke, P. Platen, and M. Kohl-Bareis, "Tissue oxygenation during exercise measured with NIRS: a quality control study," I. Georgakoudi, J. Popp, and K. Svanberg, eds., (SPIE, Munich, Germany, 2009), pp. 736816.
4. D. E. Myers, L. D. Anderson, R. P. Seifert, J. P. Ortner, C. E. Cooper, G. J. Beilman, and J. D. Mowlem, "Noninvasive method for measuring local hemoglobin oxygen saturation in tissue using wide gap second derivative near-infrared spectroscopy," J. Biomed. Opt. **10**(3), 034017 (2005).
5. Y. Yang, O. Soyemi, P. J. Scott, M. R. Landry, S. M. Lee, L. Stroud, and B. R. Soller, "Quantitative measurement of muscle oxygen saturation without influence from skin and fat using continuous-wave near infrared spectroscopy," Opt. Express **15**(21), 13715–13730 (2007).
6. Y. Teng, H. Ding, L. Huang, Y. Li, Q. Shan, D. Ye, H. Ding, J. Chien, and B. Hwang, "Non-invasive measurement and validation of tissue oxygen saturation covered with overlying tissues," Prog. Nat. Sci. **18**(9), 1083–1088 (2008).
7. G. A. Breit, J. H. Gross, D. E. Watenpaugh, B. R. I. T. Chance, and A. R. Hargens, "Near-infrared spectroscopy for monitoring of tissue oxygenation of exercising skeletal muscle in a chronic compartment syndrome model," J. Bone Joint Surg. Am. **79**(6), 838–843 (1997).
8. F. Costes, F. Prieur, L. Féasson, A. Geyssant, J. C. Barthélémy, and C. Denis, "Influence of training on NIRS muscle oxygen saturation during submaximal exercise," Med. Sci. Sports Exerc. **33**(9), 1484–1489 (2001).
9. S. Shimizu, F. Chiarotti, M. Ferrari, A. Kagaya, V. Quaresima, S. Homma, and K. Azuma, "Calf and shin muscle oxygenation patterns and femoral artery blood flow during dynamic plantar flexion exercise in humans," Eur. J. Appl. Physiol. **84**(5), 387–394 (2001).
10. D. H. Glaister, and F. F. Jöbsis-VanderVliet, "A near-infrared spectrophotometric method for studying brain O2 sufficiency in man during +Gz acceleration," Aviat. Space Environ. Med. **59**(3), 199–207 (1988).

#132403 - $15.00 USD Received 27 Jul 2010; revised 21 Aug 2010; accepted 25 Aug 2010; published 30 Aug 2010

11. L. D. Tripp, J. S. Warm, G. Matthews, P. Y. Chiu, and R. B. Bracken, "On tracking the course of cerebral oxygen saturation and pilot performance during gravity-induced loss of consciousness," Hum. Factors **51**(6), 775–784 (2009).
12. D. T. Delpy, M. Cope, P. Zee, S. Arridge, S. Wray, and J. Wyatt, "Estimation of optical pathlength through tissue from direct time of flight measurement," Phys. Med. Biol. **33**(12), 1433–1442 (1988).
13. S. Suzuki, S. Takasaki, T. Ozaki, and Y. Kobayashi, "Tissue oxygenation monitor using NIR spatially resolved spectroscopy," in *Optical Tomography and Spectroscopy of Tissue III,* Britton Chance, Robert R.Alfano, and Bruce J.Tromberg, eds., (1999), pp. 582–592.
14. S. J. Matcher, P. J. Kirkpatrick, K. Nahid, M. Cope, and D. T. Delpy, "Absolute quantification methods in tissue near-infrared spectroscopy," B. Chance and R. R. Alfano, eds., (SPIE, San Jose, CA, USA, 1995), pp. 486–495.
15. S. Fantini, D. Hueber, M. A. Franceschini, E. Gratton, W. Rosenfeld, P. G. Stubblefield, D. Maulik, and M. R. Stankovic, "Non-invasive optical monitoring of the newborn piglet brain using continuous-wave and frequency-domain spectroscopy," Phys. Med. Biol. **44**(6), 1543–1563 (1999).
16. H. Liu, D. A. Boas, A. G. Yodh, and B. Chance, "Determination of optical properties and blood oxygenation in tissue using continuous NIR light," Phys. Med. Biol. **40**(11), 1983–1993 (1995).
17. M. S. Patterson, B. Chance, and B. C. Wilson, "Time resolved reflectance and transmittance for the non-invasive measurement of tissue optical properties," Appl. Opt. **28**(12), 2331–2336 (1989).
18. S. Fantini, M. A. Franceschini, J. S. Maier, S. A. Walker, B. B. Barbieri, and E. Gratton, "Frequency-domain multichannel optical detector for noninvasive tissue spectroscopy and oximetry," Opt. Eng. **34**(1), 32–42 (1995).
19. A. A. Stratonnikov, and V. B. Loschenov, "Evaluation of blood oxygen saturation in vivo from diffuse reflectance spectra," J. Biomed. Opt. **6**(4), 457–467 (2001).
20. Y. Yang, M. R. Landry, O. O. Soyemi, M. A. Shear, D. S. Anunciacion, and B. R. Soller, "Simultaneous correction of the influence of skin color and fat on tissue spectroscopy by use of a two-distance fiber-optic probe and orthogonalization technique," Opt. Lett. **30**(17), 2269–2271 (2005).
21. S. Kirkpatrick, C. D. Gelatt, Jr., and M. P. Vecchi, "Optimization by simulated annealing," Science **220**(4598), 671–680 (1983).
22. V. Černý, "Thermodynamical approach to the traveling salesman problem: An efficient simulation algorithm," J. Optim. Theory Appl. **45**(1), 41–51 (1985).
23. H. J. van Staveren, C. J. M. Moes, J. van Marie, S. A. Prahl, and M. J. C. van Gemert, "Light scattering in Intralipid-10% in the wavelength range of 400-1100 nm," Appl. Opt. **30**(31), 4507–4514 (1991).
24. Network for translational research optical imaging and Beckman Laser Institute & Medical Clinic, University of California - Irvine, "Appendix: Tissue Phantom Recipes," in *http://www.bli.uci.edu/ntroi/pubs/pdf/phantomrecipes.pdf,* (2008).
25. K. Levenberg, "A method for the solution of certain problems in least squares," Q. Appl. Math. **2**, 164–168 (1944).
26. D. W. Marquardt, "An Algorithm for Least-Squares Estimation of Nonlinear Parameters," J. Soc. Ind. Appl. Math. **11**(2), 431–441 (1963).
27. S. J. Matcher, C. E. Elwell, C. E. Cooper, M. Cope, and D. T. Delpy, "Performance comparison of several published tissue near-infrared spectroscopy algorithms," Anal. Biochem. **227**(1), 54–68 (1995).
28. S. J. Matcher, M. Cope, and D. T. Delpy, "Use of the water absorption spectrum to quantify tissue chromophore concentration changes in near-infrared spectroscopy," Phys. Med. Biol. **39**(1), 177–196 (1994).
29. Biomedical optics laboratory, University of London. Specific extinction spectra of tissue chromophores. http://www.medphys.ucl.ac.uk/research/borl/research/NIR_topics/spectra/spectra.htm. 2005.
30. S. Luke, Essentials of Metaheuristics, available at http://cs.gmu.edu/~sean/book/metaheuristics/, 2009.
31. V. Granville, M. Krivanek, and J.-P. Rasson, "Simulated Annealing: A Proof of Convergence," IEEE Trans. Pattern Anal. Mach. Intell. **16**(6), 652–656 (1994).
32. Open source Matlab code of the SA method, http://www.mathworks.com/matlabcentral/fileexchange/10548, 2008.
33. T. J. Farrell, M. S. Patterson, and B. Wilson, "A diffusion theory model of spatially resolved, steady-state diffuse reflectance for the noninvasive determination of tissue optical properties in vivo," Med. Phys. **19**(4), 879–888 (1992).
34. C. R. Simpson, M. Kohl, M. Essenpreis, and M. Cope, "Near-infrared optical properties of ex vivo human skin and subcutaneous tissues measured using the Monte Carlo inversion technique," Phys. Med. Biol. **43**(9), 2465–2478 (1998).
35. R. Cubeddu, A. Pifferi, P. Taroni, A. Torricelli, and G. Valentini, "A solid tissue phantom for photon migration studies," Phys. Med. Biol. **42**(10), 1971–1979 (1997).
36. A. Savitzky, and M. J. E. Golay, "Smoothing and Differentiation of Data by Simplified Least Squares Procedures," Anal. Chem. **36**(8), 1627–1639 (1964).
37. C. A. Andersson, "Direct orthogonalization," Chemom. Intell. Lab. Syst. **47**(1), 51–63 (1999).
38. J. Martin Bland, and D. Altman, "Statistical methods for assessing agreement between two methods of clinical measurement," Lancet **327**(8476), 307–310 (1986).
39. L. F. Ferreira, D. M. Hueber, and T. J. Barstow, "Effects of assuming constant optical scattering on measurements of muscle oxygenation by near-infrared spectroscopy during exercise," J. Appl. Physiol. **102**(1), 358–367 (2006).

#132403 - $15.00 USD Received 27 Jul 2010; revised 21 Aug 2010; accepted 25 Aug 2010; published 30 Aug 2010

40. S. Homma, T. Fukunaga, and A. Kagaya, "Influence of adipose tissue thickness on near-infrared spectroscopic signal in the measurement of human muscle," J. Biomed. Opt. **1**(4), 418–426 (1996).
41. M. C. van Beekvelt, M. S. Borghuis, B. G. van Engelen, R. A. Wevers, and W. N. Colier, "Adipose tissue thickness affects in vivo quantitative near-IR spectroscopy in human skeletal muscle," Clin. Sci. **101**(1), 21–28 (2001).
42. A. Kienle, M. S. Patterson, N. Dögnitz, R. Bays, G. Wagnivres, and H. van den Bergh, "Noninvasive Determination of the Optical Properties of Two-Layered Turbid Media," Appl. Opt. **37**(4), 779–791 (1998).

1. Introduction

Near infrared spectroscopy (NIRS) has been used to determine *in vivo* tissue oxygen saturation (StO_2), for a number of diverse and important research and clinical applications [1–11]. NIR light, typically in the wavelength region between 700 and 1000*nm*, penetrates skin, fat and skull to illuminate underlying tissue, such as the muscle and the brain. Photons are both absorbed and scattered within the tissue. A portion of the photons have trajectories that allow them to reach an external detector for analysis after they have passed through the tissue. The relatively high attenuation of NIR light within tissue results from absorbance of chromophores, such as oxygenated and deoxygenated hemoglobin (HbO_2 and Hb, respectively) in blood, melanin in skin, as well as light scattering from skin, fat and tissue (muscle or brain). Blood oxygen saturation is defined as $SO_2 = c_{HbO_2} / (c_{HbO_2} + c_{Hb}) 100\%$, where c_{HbO_2} and c_{Hb} are the concentrations of oxygenated and deoxygenated hemoglobin, respectively, which have characteristic absorbance bands in this region of the NIR spectrum.

When considering pure absorbance, the Beer-Lambert law states that the light attenuation by an analyte dissolved into a nonscattering solvent is linearly related to the product of the concentration of the analyte and the optical pathlength. If the analyte is present in a scattering medium, such as tissue, the physical pathlength of the photons is larger than the geometrical distance between the light source and detector because of multiple scattering events. The effect of scattering on the spectral baseline is sometimes described with a modified Beer-Lambert law equation where a term G is added [12]. An absolute determination of StO_2 requires a method to determine both the effective pathlength of photons in tissue, as well as the effect of scattering on the spectral baseline.

Historically, a variety of different approaches have been used to address the effect of light scattering in tissue for the absolute determination of tissue oxygen saturation. Spatially resolved spectroscopic (SRS) methods, based on either broadband or discrete wavelengths, have been reported. These methods use the diffusion approximation model and at least two source-detector distances [13–16]. Time-resolved spectroscopy (TRS) [17] and phase or frequency modulation spectroscopy (PMS) [18] can resolve absolute absorbance and scattering and hence calculate StO_2 through the time of flight of photons, or from modulated light information, respectively. Continuous-wave (CW) NIRS (CW-NIRS) is the simplest and most cost effective technique for real-time clinical monitoring of patients. Recent efforts have attempted to use non-spatially resolved CW instruments to measure absolute StO_2. Myers, Anderson, and Seifert *et al* [4] employed a 4 wavelength "wide gap" second derivative spectroscopic method to remove the effect of scattering by producing an StO_2 calibration curve which related scaled second derivative attenuation at 720*nm* to hemoglobin SO_2 from *in vitro* hemoglobin samples. This technique is limited since the scattering properties of *in vivo* tissue are different from the *in vitro* hemoglobin samples used to produce the calibration curve. Stratonnikov and Loschenov [19] proposed a non-spatially resolved CW spectroscopic technique to measure absolute StO_2 using visible light by employing a Taylor expansion attenuation model. This algorithm is simple and robust and was successfully employed in the wavelength region 510 to 590*nm*, where oxygenated and deoxygenated hemoglobin have sharp absorbance bands. In their hands, this approach was unsuccessful in the NIR wavelength range. Neither did their method account for spectral interference from skin

#132403 - $15.00 USD Received 27 Jul 2010; revised 21 Aug 2010; accepted 25 Aug 2010; published 30 Aug 2010

pigment or fat. Modifications of this method are required for routine clinical application to determine StO_2 in underlying tissues.

Yang *et al* have previously shown that the method of Stratonnikov and Loschenov [19] can be successfully adapted to the NIR region [5], where light can penetrate deeper inside the tissue. This method first removed the spectral interference of light absorbance and scattering from the skin pigment and fat using a dual-source, single detector method [20]. Subsequently a nonlinear least-square fit was used to determine HbO_2, Hb, and in turn StO_2 from the muscle-only spectrum.

The accuracy of any algorithm for determining StO_2 from CW-NIR spectra depends upon methods for estimating the contribution of light scattering. The attenuation model described in this paper uses a linear term to model the tissue scattering component of the optical attenuation. While scattering effects contribute significantly to the spectral baseline, other tissue components and the optical system design can also affect the spectrum, and in turn the accuracy of StO_2 determination. These factors include the concentration of hemoglobin in blood, the volume of blood and water in the tissue under the sensor, fat thickness, and the source-detector (S-D) spacing. An StO_2 monitor targeted toward application in the care of critically ill patients must be able to accurately determine StO_2 when blood volume under the sensor may change, through vasodilation or vasoconstriction, which occurs independently of changes in hemoglobin concentration. During treatment of trauma patients, large volumes of non-blood fluids are often employed, rapidly changing the fraction of water in the tissue.

Recently we have improved the performance of our algorithms for calculating StO_2 by simplifying the mathematical model used in the Taylor expansion and employed the simulated annealing (SA) method [21,22] to initialize the least square fit of the measured spectrum and attenuation model. The SA method was employed to improve the precision of the initialization step. The aims of this study are to assess StO_2 prediction accuracy of the updated algorithm on a set of simulated spectra which were constructed to independently vary S-D spacing, total hemoglobin concentration, and water volume. The algorithm was further validated on a dual-dye phantom model simulating the absorbance spectra of varying levels of SO_2 through the use of two dyes with absorbance peaks similar to oxygenated and deoxygenated hemoglobin. The aims of the phantom study are to determine dye ratio, an analog of StO_2, prediction accuracy of the updated algorithm under conditions of varying fat thickness, absorber volume, and total absorber concentration.

2. Materials and methods

2.1 StO_2 prediction model

According to light diffusion theory, the tissue attenuation spectrum is expressed as the natural logarithm of the ratio of incident light intensity (I_0) to reflected light intensity (I). In our application, I_0 is estimated as the reflected light intensity from a 99% reflectance standard, I_{ref} , when calculating measured light attenuation spectra. I_{ref} differs from I_0 by a wavelength independent constant, c, resulting in the appearance of an additive constant in the experimental attenuation curve. Beer's law describes a relationship between the concentration of the absorbers, and the incident and reflected light intensity. The measured light attenuation spectrum, $A_{\text{exp}}(\lambda)$ is generalized to simplify and accelerate computer processing to calculate the concentration of oxygenated and deoxygenated hemoglobin [Eq. (1)] as follows:

$$\begin{aligned} A_{\text{exp}}(\lambda) &= \ln\frac{I_{\text{ref}}(\lambda)}{I(\lambda)} = \ln\frac{I_0(\lambda)}{I(\lambda)} + c \\ &= c_0 + c_1\mu'_{\text{s},0}(\lambda) + \langle \text{L} \rangle [c_{\text{Hb}}\varepsilon_{\text{Hb}}(\lambda) + c_{\text{HbO}_2}\varepsilon_{\text{HbO}_2}(\lambda)]\ln 10 + c_{\text{H}_2\text{O}}\varepsilon_{\text{H}_2\text{O}}(\lambda)\ln 10 + \text{error}, \end{aligned} \tag{1}$$

#132403 - $15.00 USD Received 27 Jul 2010; revised 21 Aug 2010; accepted 25 Aug 2010; published 30 Aug 2010

where c_0 and c_1 are constants, $\mu'_{s,0}(\lambda)$ is the reduced scattering function of 0.8% Intralipid [23,24] normalized to $1cm^{-1}$ at $800nm$, $\langle L \rangle$ is the average pathlength of the reflected light through the tissue, c_{Hb} and c_{HbO_2} are the concentration of deoxygenated hemoglobin (Hb) and oxygenated hemoglobin (HbO_2), respectively, c_{H_2O} is a function of the water fraction and average pathlength in the tissue, $\varepsilon_{Hb}(\lambda)$, $\varepsilon_{HbO_2}(\lambda)$, and $\varepsilon_{H_2O}(\lambda)$ are the wavelength dependent extinction coefficients of Hb, HbO_2, and H_2O, respectively. Equation (1) is similar to Yang *et al*'s prediction model [5] except that the term describing light scattering is given a wavelength dependence proportional to the scattering coefficient for Intralipid, to better model scattering from muscle tissue. Additionally the pathlength attributable to water absorbance is merged with the estimation of water fraction in tissue. This modification simplifies the mathematics and helps speed up the processing time, which is important for employing the model in real time.

Typically, light attenuation in the target tissue arises from both light absorbance and light scattering processes. Light is absorbed by hemoglobin and myoglobin, by both intravascular and extravascular water, and by melanin pigment in skin. Light can be scattered by physical structures such as blood vessel walls and muscle fibers, and by fat which overlies the muscle tissue. In our application, the component of the spectrum resulting from skin pigment and fat scattering is removed by using a two-source, one-detector configuration fiber optic probe [20]. The attenuation spectrum collected with the long S-D distance ($3.0cm$) pair is orthogonalized by the one collected with the short S-D distance ($0.25cm$) pair. The resultant spectrum describes the attenuation from only the muscle layer [20]. Unpublished studies in our laboratory have demonstrated this source-detector pair is effective in removing fat layers up to 8mm in thickness. Then the nonlinear least square (LSQ) method is initialized with the first spectrum using the SA method (see Section 2.2), to find the optimal initial values for all six parameters, i.e., c_0, c_1, $\langle L \rangle$, c_{Hb}, c_{HbO_2}, and c_{H_2O}. The nonlinear LSQ method uses the Levenberg-Marquardt algorithm [25,26] to optimize Eq. (1) and is implemented with "lsqcurvefit" function in the Matlab® Optimization Toolbox (version 3.0.2) (Mathworks Inc., Natick, MA). The extinction coefficients of Hb, HbO_2, and water are linearly interpolated from those measured by Matcher *et al* [27–29] to match our spectrometer's wavelength resolution and used in the SO_2 algorithm.

With the calculated values c_{Hb} and c_{HbO_2}, StO_2 is determined as follows:

$$StO_2 = \frac{c_{HbO_2}}{HbT} 100\%, \tag{2}$$

where $HbT = c_{Hb} + c_{HbO_2}$, is the total hemoglobin concentration.

2.2 Initialization using the simulated annealing method

In the Taylor StO_2 prediction model, one initial value for each of the six parameters is required. When the algorithm is implemented the initial value for each parameter is determined from the first spectrum that is collected from the patient. Yang *et al* [5] used the "sweeping method" on the variables slope, baseline, and pathlength, while setting the variables of c_{Hb}, c_{HbO_2}, and c_{wat} (water fraction) to a normal baseline value. This method works well on healthy human subjects; however, for patients with abnormal condition when the first reading is taken, the actual values for c_{Hb} and c_{HbO_2} could be far from the value used to initiate the fit between the measured spectrum and the model. With the nonlinear LSQ, which is used to determine c_{Hb} and c_{HbO_2}, as well as other parameters, the values used to initiate the calculation have a significant effect on the accuracy of the StO_2 determination. In this paper, the SA method is implemented to determine the initial values of all the six

#132403 - $15.00 USD Received 27 Jul 2010; revised 21 Aug 2010; accepted 25 Aug 2010; published 30 Aug 2010

parameters. The SA method is an efficient method for optimization of the large class of the NP-complete (nondeterministic polynomial time complete) problems.

SA is a generic probabilistic metaheuristic [30] method with user-provided procedures for the global optimization problem of applied mathematics, namely locating a good approximation to the global optimum of a given function in a large search space. In the SA method, each point *p* of the search space is analogous to a state of some physical system, and the function E(*p*) to be minimized (called a loss function) is analogous to the internal energy of the system in that state. The goal is to bring the system, from an arbitrary initial state, to a state with the minimum possible energy. Granville *et al* [31] proved that for any given finite problem, the probability that the SA algorithm terminates with the global optimal solution approaches 1 as the annealing schedule is extended.

We suggest that by employing the SA method we can identify initial values that consistently produce accurate values for StO_2 no matter what the SO_2 value actually is for the first spectrum. We used an open source implementation of the SA method in Matlab [32] to find a global minimum for the six variables where the loss function is defined as the square error of the actual spectrum and the one calculated with Eq. (1) in a bounded region. In our implementation, we separated the bounded region of the variables into five sub-regions. Initial values were determined with the SA method in each sub-region and the set of initial values with the smallest fit error with the initial spectrum was selected.

2.3 Calculation of simulated spectra

A set of simulated spectra were calculated using the method described by Farrell *et al* [33]. For a single scatter source, the diffuse reflectance *R* at distance ρ between a light source and a detector is as follows:

$$\begin{aligned} R(\rho) &= \int_0^\infty R(\rho, z_0)\,\delta\left(z_0 - \frac{1}{\mu'_t}\right) dz_0 \\ &= \frac{a'}{4\pi}\left[\frac{1}{\mu'_t}\left(\mu_{eff} + \frac{1}{r_1}\right)\frac{e^{-\mu_{eff} r_1}}{r_1^2} + \left(\frac{1}{\mu'_t} + 2z_b\right)\left(\mu_{eff} + \frac{1}{r_2}\right)\frac{e^{-\mu_{eff} r_2}}{r_2^2}\right], \end{aligned} \tag{3}$$

where $\mu_{eff} = [3\mu_a(\mu_a + \mu'_s)]^{1/2}$ is the effective attenuation coefficient, $a' = \mu'_s/(\mu_a + \mu'_s)$ is the transport albedo, $\mu'_t = \mu_a + \mu'_s$ is the total interaction coefficient, z_b and r_i (i = 1, 2) are defined in that paper. Then the absorbance is as follows:

$$A(\rho) = -\ln(R(\rho)), \tag{4}$$

To validate the SO_2 prediction model [Eq. (1)], in which the SA method is used, a set of simulated absorbance spectra were generated using above model [Eq. (3)], in which μ_a consists of Hb, HbO_2, and H_2O components. The considered parameters are listed in Table 1.

Table 1. Parameter values used to generate the simulates spectra

Parameter	Value
SO_2 (%)	90, 80, 70, 60, 50, 40, 30, 20, 10, 5
HbT(*mM*)	0.08, 0.1, 0.12
H_2O (volume fraction)	0.6, 0.7, 0.8
μ_s' (at 800*nm*) (cm^{-1})	5, 7
S-D distance (*cm*)	3.0, 4.0, 5.0

The simulated spectra of S-D distance of 3.0*cm* are shown in Fig. 1(a):

#132403 - $15.00 USD Received 27 Jul 2010; revised 21 Aug 2010; accepted 25 Aug 2010; published 30 Aug 2010

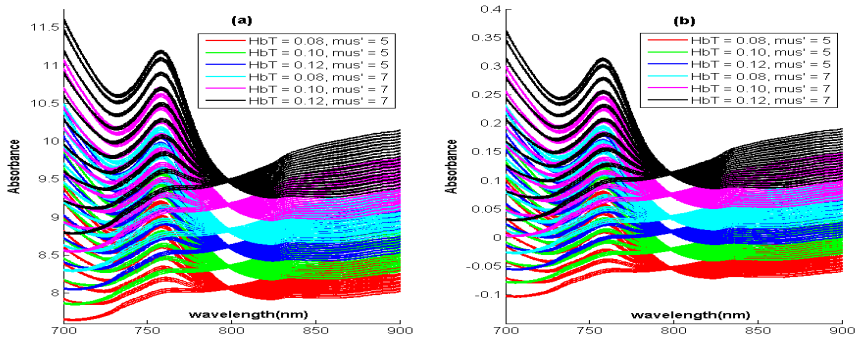

Fig. 1. Farrell [33] simulated spectra using parameters of SO_2 = 90, 80, 70, 60, 50, 40, 30, 20, 10, 5; HbT = 0.08, 0.1, 0.12*mM*; H_2O = 0.6, 0.7, 0.8; μ_s' = 5, 7cm^{-1}. (a) With S-D of 3.0*cm*; (b) after an affine transformation.

In our evaluation of simulated and phantom spectra an affine transform was used to transform the spectra into the interval of (−1, 1) prior to calculation of SO_2. The reason that an affine transformation was performed is to meet the requirement of the Taylor expansion. The affine transformation, $y = ax + b$, consists of a scaling and a translation. A simple calculus shows that the affine transformation does not change the SO_2 calculation since it is a ratio, although it does affect the absolute value of c_{Hb} and $c_{\mathrm{HbO_2}}$. The simulated spectra after an affine transform are depicted in Fig. 1(b).

2.4 Dual-dye phantoms for studying the effect of fat thickness and blood volume

A set of dye phantoms were also made to validate the method for determining StO_2. Two NIR dyes with distinct absorbance peaks were used to simulate the tissue chromophores. One dye (denoted as Dye1, ADS780WS, American Dye Source, Inc., Quebec) has maximal absorption at 780nm in methanol; The other dye (denoted as Dye2, Epolight5588, Epolin, Inc., Newark, NJ) exhibits maximal absorption at 860nm in methanol. The extinction coefficients of both NIR dyes are illustrated in Fig. 2. They have similar absorptivity in terms of light attenuation in unit concentration per centimeter which makes it fairly straightforward to combine the two dyes to simulate SO_2 absorbance.

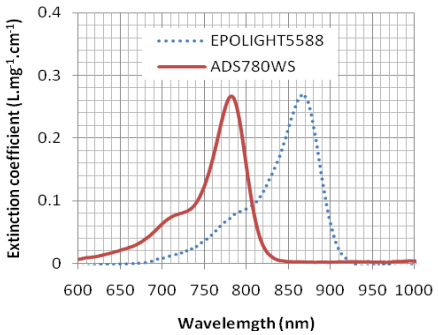

Fig. 2. Absoroption spectra of NIR dyes in methanol.

Five mixtures of these two dyes were prepared in methanol so that their compositions ([Dye1]:[Dye2] in $\mu g/mL$) are 4:0, 3:1, 2:2, 1:3 and 0:4, respectively. This set of data is denoted as DyeCC4. The total concentration of dyes was kept constant at 4$\mu g/mL$, while the ratio d_{Ratio} of Dye2, which is defined as

#132403 - $15.00 USD Received 27 Jul 2010; revised 21 Aug 2010; accepted 25 Aug 2010; published 30 Aug 2010

$$d_{Ratio} = \frac{[\text{Dye2}]}{[\text{Dye1}]+[\text{Dye2}]}100\%, \text{ where } [\text{Dye}] \text{ represents Dye concentration,} \quad (5)$$

varied from 0%, 25%, 50%, 75% to 100%. Another series of five dye mixtures were also prepared in methanol with the same relative compositions but a different total concentration of $3\mu g/mL$. This set of data is denoted as DyeCC3. Dye mixture solutions of these known compositions were used to fill capillary tubes (length = $12.0cm$; inner diameter = $1.3mm$; outer diameter = $2.2mm$) and the filled tubes were sealed on both ends with clay. For DyeCC4, a total of 10, 9, and 8 tubes were placed side-by-side on the top of the 99% Spectralon reference standard (99% reflectance, Spectralon, Labsphere, Inc., New Sutton, NH). For DyeCC3, a total of 10 tubes were placed side-by-side on the top of the standard. These tubes were covered with a simulated fat layer of varying thicknesses ($4.0mm$, $6.0mm$, and $8.0mm$). The fat layer was topped with a $1.0mm$ layer of simulated skin of medium color.

The nominal reduced scattering coefficient (μ_s') of the fat and skin layer phantoms at $800nm$ were $12cm^{-1}$ and $15cm^{-1}$, respectively [34]. The fabrication of the skin and fat layer phantoms followed the procedure described by Cubeddu *et al* [35]. The solid fat layer was constructed of 6 volume percent Intralipid (20%, Baxter Healthcare Corp., Deerfield, IL), 1% by weight agar (A7921, Sigma-Aldrich, Co., St. Louis, MO), and 94% (volume percent) distilled water); the solid skin layer consisted of 15 volume percent $0.15mg/mL$ melanin (M8631, Sigma-Aldrich Co., St. Louise, MO), 7.5 volume percent Intralipid (20%), 1% by weight agar, and 77.5 volume percent distilled water.

Spectral measurements were recorded with the previously described fiber optic system [5,20], with the fiber optic probe placed directly on the top of the skin layer. This system employs a two-distance fiber-optic probe with two source bundles and one detector bundle. At the probe head, the distance of the "short" source bundle from the detector (SD1) is small enough that the detector bundle detects the light that has penetrated only the skin and fat layers. The spacing of the "long" bundle from the detector bundle (SD2) is long enough that the detector bundle acquires the light that has penetrated through the skin, fat and muscle layers. For the system used to measure dye phantom spectra, the distance of the short bundle from the detector is $0.25cm$, and the distance of the long bundle from the detector is $3.0cm$. The detector bundle is connected to an Ocean Optics VIS-NIR spectrometer (Model USB2000, Dunedin, FL). The source bundles are connected to a tungsten lamp via an on-axis, large-diameter connector and an off-axis, smaller-diameter connector, respectively. A computer-controlled shutter switches between the two source bundles to allow only one source bundle to be illuminated by the lamp at a time. Reflectance of each phantom was measured by sequential illumination with the short and long distance light sources. Spectra were converted to absorbance by referencing to a 99% reflectance standard placed a fixed distance below the sensor, and then both the long distance and short distance spectra were smoothed by the Savitsky-Golay smoothing method [36]. As discussed previously [20], orthogonalization of the short to long spectra were done with Andersson's method [37].

Figure 3 depicts the 60 dye phantom long distance attenuation spectra (a), the orthogonalized spectra by the short-distance attenuation spectra (b), and the orthogonalized spectra after an affine transformation (c).

#132403 - $15.00 USD Received 27 Jul 2010; revised 21 Aug 2010; accepted 25 Aug 2010; published 30 Aug 2010

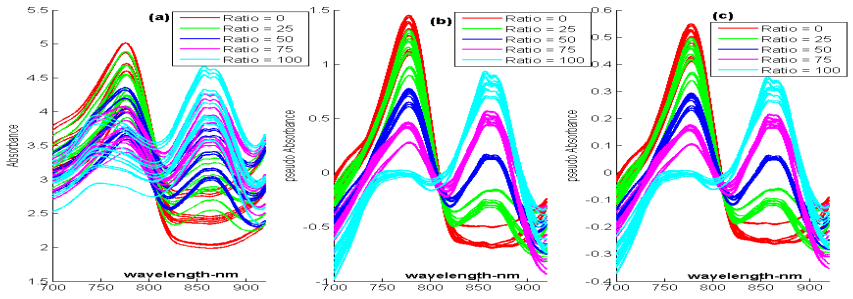

Fig. 3. Sixty dye phantom spectra. (a) Long S-D distance absorbance spectra; (b) orthogonalized spectra; (c) orthogonalized spectra after an affine transformation.

From the orthogonalized spectra after an affine transformation [Fig. 3(c)], we randomly select one spectrum as the first one and determine the initial values for the nonlinear LSQ step. The dye concentration is predicted using an analog of the SO_2 prediction model [Eq. (1)], where the extinction coefficients of Hb and HbO_2 are replaced with those of Dye1 and Dye2 respectively. Then dye ratio [defined in Eq. (5)] is calculated as an analog for SO_2.

2.5 Data analysis

SO_2 was calculated for the 540 simulated spectra which were generated using the values for the parameters in Table 1. Accuracy was assessed by calculating the coefficient of determination (R^2) and the root mean squared error of prediction (RMSEP) between the set SO_2 value and that determined with our algorithm. The RMSEP is calculated according to Eq. (6):

$$\mathrm{RMSEP} = \sqrt{\frac{\sum_{i=1}^{N} (\hat{y}_i - y_i)^2}{N}}, \tag{6}$$

where N is the number of light attenuation spectra, and $\hat{y}_i$ and y_i are the predicted and actual SO_2 values, respectively (i = 1, 2, …, N). $R^2 = 1$ and RMSEP = 0 means perfect matching. The results are analyzed separately to demonstrate the effect of S-D spacing, total hemoglobin concentration (HbT), scattering coefficient of the muscle (μ_s') and water.

Additionally, accuracy was assessed for the 60 phantom spectra by calculating R^2 and RMSEP for the actual and predicted dye ratios. The effect of total dye concentration, an analog for variation in total hemoglobin concentration; number of tubes, an analog for blood volume under the sensor; and fat thickness are presented in separate graphs.

The accuracy of the algorithm for the prediction of StO_2 was also compared to the known values for both simulated and phantom spectra using the method of Bland and Altman [38]. With this method, the bias describes the mean difference between the actual and predicted measurements. The limits of agreement are defined as the mean difference plus or minus 1.96 times the standard deviation of the differences.

The effect of the initial spectrum on accuracy was assessed by comparing the predicted accuracy of the algorithm when different values of SO_2 were used as the starting point. For this test, the 180 simulated spectra of S-D spacing of 4.0*cm* were used. For these 180 spectra, for each HbT, μ_s', and water, we selected the spectrum with SO_2 = 60, 30, 10, 90, as the first spectrum to find a set of initial values with the SA method, providing 72 different sets of initial values. Each set of these initial values was then used to predict SO_2 from the set of 180 spectra and calculate the estimated error (RMSEP) resulting from variation in starting condition.

#132403 - $15.00 USD Received 27 Jul 2010; revised 21 Aug 2010; accepted 25 Aug 2010; published 30 Aug 2010

3. Results and discussion

3.1 Accuracy results from simulated spectra

Long distance source and detector (S-D) separation can have a significant effect on the accuracy of StO_2 determination. We determined that separate initial value calculations must be done for each long distance S-D, i.e. initial values determined for a sample assuming a long S-D of 3.0*cm* were not appropriate for spectra of the same sample with an S-D of 4.0*cm* . For each of the three S-D separations studied, we randomly selected one spectrum from the 180 simulated spectra (after an affine transformation) as the first spectrum to search a set of initial values with the SA method. SO_2 values were calculated from the 180 spectra collected at each S-D distance. Figure 4 illustrates the actual and predicted values of SO_2, with the specific values for R^2 and RMSEP as a function of S-D detailed in Table 2. There is good agreement between the actual and predicted SO_2 values, with the estimated error (RMSEP) increasing as S-D increases. This result is not unexpected since as the S-D distance increases signal-to-noise ratio decreases as a result of increased absorbance and scattering over the longer distance.

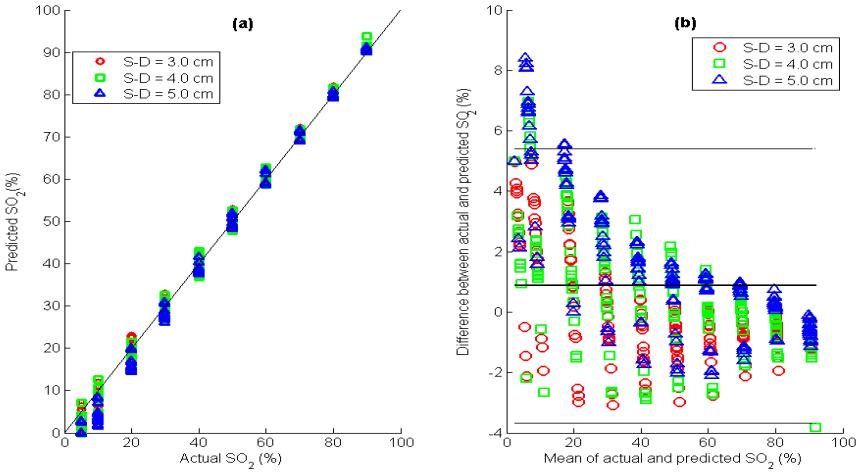

Fig. 4. Plots of SO_2 results from 540 simulated spectra with different long S-D distances. (a) Predicted vs actual SO_2, the diagonal line represents perfect prediction; (b) Bland and Altman plot of actual and predicted SO_2, in which the bias is 0.87%, the standard deviation of the difference is 2.31%.

Table 2. R^2 and RMSEP for the predicted SO_2 results from simulated spectra with different S-D distances

S-D distance (*cm*)	R^2	RMSEP (% SO_2)
3.0	0.997	1.87
4.0	0.996	2.34
5.0	0.997	3.05

#132403 - $15.00 USD Received 27 Jul 2010; revised 21 Aug 2010; accepted 25 Aug 2010; published 30 Aug 2010

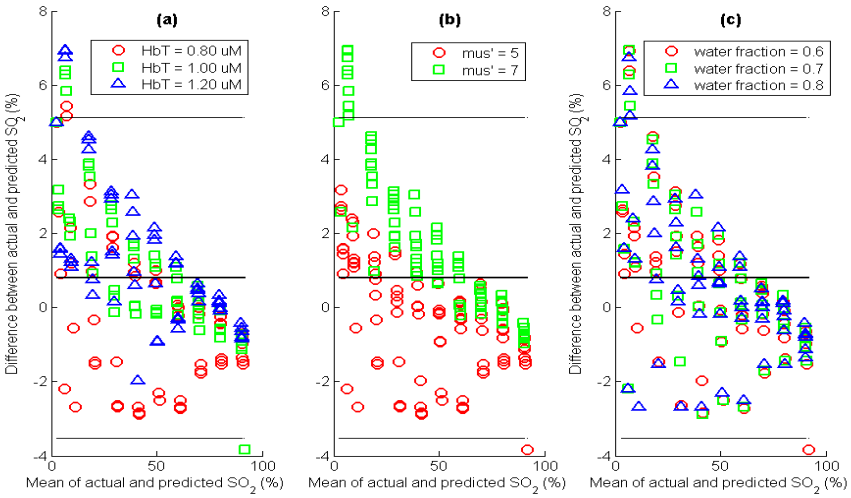

Fig. 5. Bland-Altman plots of actual and predicted SO_2 results from simulated spectra with S-D distance of 4.0*cm*. (a) Relation with varying HbT; (b) relation with varying μ_s'; (c) relation with different water fraction.

To evaluate the effect of varying HbT, muscle μ_s', and water fraction on the accuracy of our SO_2 calculation algorithm, we present only the simulated spectra with S-D distance of 4.0*cm* (Fig. 5 and Table 3); results are similar for the other S-D distances. In this set of simulated data RMSEP is similar for each tested value of HbT and water volume fraction. Calculation accuracy may be influenced by μ_s'. When μ_s' is $5cm^{-1}$, RMSEP is 1.56%; RMSEP increases to 2.92% with a μ_s' of $7cm^{-1}$. Ferreira *et al* [39] have previously shown that it is important to account for variation in μ_s' when calculating StO_2 in a setting such as exercise, that will alter μ_s' over a series of measurements. In their study an increase in μ_s' from $6cm^{-1}$ to $7cm^{-1}$ (at 690*nm*) during exercise resulted in a StO_2 error of 7% at peak exercise, when values for μ_s' were not updated. In our implementation we redetermine a value for μ_s' with each spectrum, therefore we adjust μ_s' as optical variation warrants. Our simulation showed that while a change from $5cm^{-1}$ to $7cm^{-1}$ increased our error, the StO_2 error at the higher scattering coefficient was still less than 3% (Table 3).

Table 3. R^2 and RMSEP for the predicted SO_2 results from simulated spectra with S-D distance of 4.0*cm*, with different factors

Factor	Value	R^2	RMSEP (% SO_2)
HbT (μM)	0.1	0.998	2.36
	0.08	0.996	2.16
	0.12	0.997	2.49
μ_s' (cm^{-1})	5	0.998	1.56
	7	0.999	2.92
Water volume fraction	0.6	0.997	2.26
	0.7	0.997	2.38
	0.8	0.996	2.37
overall		0.996	2.34

The data show that despite significant variation in water volume fraction, there is good accuracy in the measurement of SO_2. There appears to be no trend in the error with water fraction. This is a significant finding for the clinical application of this technology. Edema, or water accumulation in tissue, often occurs in the periphery of critically ill patients, patients who are likely to be monitored with tissue SO_2 devices. Water has small, but significant

#132403 - $15.00 USD Received 27 Jul 2010; revised 21 Aug 2010; accepted 25 Aug 2010; published 30 Aug 2010

absorbance in the wavelength region between 700*nm* and 900*nm*. Our algorithms accurately account for this absorbance and should be suitable for monitoring patients who accumulate water in their tissues.

3.2 Accuracy results from phantom spectra

The results for dye concentration, number of tubes, and fat thickness calculated from spectra collected from the phantoms are presented in Fig. 6 and Table 4.

The estimated error (RMSEP) in the calculation of dye ratio is very small, averaging 1.4% for all samples. There is small variation in estimated accuracy between the two dye concentrations, the number of tubes and the fat thickness. In this analog system, dye concentration simulates variation in hemoglobin concentration within the blood vessels, while the number of dye tubes simulates the volume of blood in tissue which is assessed with the optical sensor. These two factors can change independently. The volume of blood analyzed is a function of the optical system and the scattering coefficient of the muscle. In tissue the scattering coefficient is determined by the density of small blood vessels and the size of the blood vessels. Both parameters can change over time as the patient's vasculature accommodates their illness and therapies are provided. In this phantom study our algorithms for calculating SO_2, adapted to calculate dye ratio, were shown to be impervious to independent variations in analogs for hemoglobin concentration and blood volume in tissue.

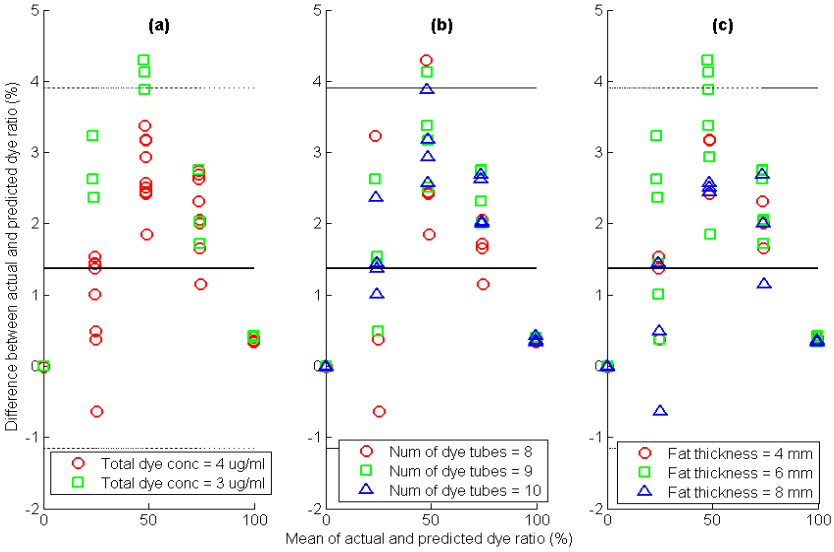

Fig. 6. Bland and Altman plots of measured and predicted dye ratio from the dye phantom spectra with different absorbance and scattering properties, in which the bias is 1.38% and the standard deviation of the difference is 1.29%. (a) Relation with varying total dye concentration; (b) relation with analog of varying total hemoglobin; (c) relation with different fat thickness.

#132403 - $15.00 USD Received 27 Jul 2010; revised 21 Aug 2010; accepted 25 Aug 2010; published 30 Aug 2010

Table 4. R^2 and RMSEP for dye ratio calculated from orthogonalized spectra of the dual-dye phantoms with different scattering and absorbance properties

	value	R^2	RMSEP (% dye ratio)
Total dye concentration ($\mu g/mL$)	3	0.999	1.90
	4	1.0	1.18
Number of dye tubes	8	0.999	1.45
	9	0.999	1.43
	10	1.0	1.31
Fat thickness (mm)	4.0	1.0	1.27
	6.0	0.999	1.60
	8.0	1.0	1.03
Overall		0.999	1.40

If not corrected, spectral interference from fat is known to cause a significant error in the estimation of StO_2 [40,41]. In this phantom model, with light sources at 0.25cm and 3.0cm, the error in the calculation of dye ratio was small and did not increase with increasing fat thickness.

3.3 Measurement precision, effect of initial value selection on repeatability

We evaluated how the StO_2 value of the initial spectrum, as well as the values of the parameters that cause spectral interference, can impact prediction from future spectra where conditions may be quite different from the initial conditions. Each of the 180 simulated spectra was evaluated with a set of 72 different starting value sets. The mean RMSEP resulting from the variation in starting conditions was 2.67% with a standard deviation of 0.38%. This value is consistent with errors calculated for all parameters with S-D of 4.0cm. The small standard deviation indicates that there is very little effect of starting conditions on the accuracy of StO_2 prediction when the SA method is used to determine the parameter values to initialize the LSQ step.

3.4 Potential limitations

In this study, we assumed that our methodology completely removes spectral contributions from the skin and fat layer. For this reason our simulations were done with the single layer diffusion theory model proposed by Farrell *et al* [33]. If the orthogonalization step did not completely eliminate the effect of fat, it would be more appropriate to use the two layer semi-infinite model proposed by Kienle *et al* [42] to test the algorithm.

Our phantom model has some limitations as well. As with the simulated spectra, we assumed complete elimination of spectral contribution from fat. Since calculated SO_2 was shown to have a small error in accuracy that did not increase with fat thickness, we assume that the assumption was valid for this study. This assumption would not be correct for thicker fat layers and might not be correct for different sensor configurations. In our phantoms, we used glass capillary tubes to represent blood vessels containing blood. These tubes are arranged next to each other on a totally reflective base of spectralon. The glass tubes might introduce light piping, which would alter the optical reflection of the system, but since SO_2 is calculated as a ratio, this effect is likely to be eliminated. Real blood vessels are not parallel and are contained in a scattering matrix. Though our phantoms did not include a base which scattered light, we did address the effect of scattering in the muscle layer with the set of 540 simulated spectra. Another limitation of the phantom model was the use of two near infrared absorbing dyes to represent oxygenated and deoxygenated hemoglobin. The dye chosen to represent oxygenated hemoglobin has an absorbance spectrum which is somewhat dissimilar to oxygenated hemoglobin, with both higher absorbance and a more defined peak. However, the simulated spectra use the actual extinction coefficients of hemoglobin. The effect of total hemoglobin (or dye concentration) on the accuracy of SO_2 (or dye ratio) calculation was examined with both the simulated spectra and the phantom. With the simulated spectra the

#132403 - $15.00 USD Received 27 Jul 2010; revised 21 Aug 2010; accepted 25 Aug 2010; published 30 Aug 2010

average estimated error over the 3 total hemoglobin concentrations was 2.34%, while with the phantoms the average estimated error was 1.54% for the two different dye concentrations. These errors are similar, considering the relative differences in the concentration range between the phantom and simulated spectral studies. Lastly, the dye used in the phantoms is that unlike blood, the dye does not include components that scatter light differently from the background, i.e. blood cells. A phantom which more closely resembles tissue would contain an agar base, with Intralipid to provide a scattering element, and tubes which contain whole blood. We are developing the methodology to construct and measure such phantoms.

4. Conclusions

This study investigated the application of a Taylor series expansion model of Beer's law on simulated muscle spectra and dual dye phantoms which incorporated skin and fat layers. A novel feature of this study is the application of the simulated annealing (SA) method to indentify initial values for the six parameters used to fit spectra for the calculation of tissue SO_2. This method was demonstrated to be highly repeatable and independent of starting conditions. Using simulated tissue spectra it was shown that this method resulted in estimated error of prediction less than 3.1% across a variety of conditions that simulate pathophysiology that can affect tissue spectra. The error was found to decrease with smaller separation between the long distance light source and detector. The estimated error from the set of 540 simulated spectra was similar for the range of total hemoglobin and water fraction studied. Two different, but physiologically relevant scattering coefficients were investigated, with prediction error found to be bigger for the larger scattering coefficient. With the dual dye phantoms it was demonstrated that dye ratio could be determined accurately with independent variation in absorber concentration and volume. Similarly, in this phantom, the estimated error was independent of the thickness of the overlying layer of fat.

The purpose of this study was to evaluate an algorithm which can be used with broadband CW-NIRS for determination of StO_2 in clinical conditions, such as trauma, where it is expected that blood volume, hemoglobin concentration and water fraction can all change rapidly in the same patient and patients can present with initial SO_2 values that are very low, far from normal conditions. The results of this investigation show promise for application of the algorithm in actual clinical scenarios, though this remains to be confirmed with actual experimental data.

Acknowledgements

This work was supported by the National Space Biomedical Research Institute (NSBRI) through NASA cooperative agreement NCC 9-58 and the US Army Medical and Materiel Research Command under contract W81XWH-08-C-0114. We'd like to acknowledge Peter J. Scott and Gwenn E. C. Ellerby for their assistance with data collection and analysis.

#132403 - $15.00 USD Received 27 Jul 2010; revised 21 Aug 2010; accepted 25 Aug 2010; published 30 Aug 2010